

CNK and HYP form a discrete dimer by their SAM domains to mediate RAF kinase signaling

Thanashan Rajakulendran^{*†}, Malha Sahmi[‡], Igor Kurinov^{§¶}, Mike Tyers^{*†}, Marc Therrien^{||**}, and Frank Sicheri^{*†**}

^{*}Centre for Systems Biology, Samuel Lunenfeld Research Institute, Toronto, ON, Canada M5G 1X5; [†]Department of Molecular Genetics, University of Toronto, Toronto, ON, Canada M5S 1A8; [‡]Institute for Research in Immunology and Cancer, Laboratory of Intracellular Signaling, Université de Montréal CP 6128, Montréal, QC, Canada H3C 3J7; [§]Department of Chemistry and Chemical Biology, Cornell University, Ithaca, NY 14853; [¶]NE-CAT, Advanced Photon Source, Argonne National Laboratory, 9700 South Cass Avenue, Argonne, IL 60439; and ^{||}Département de pathologie et de biologie cellulaire, Université de Montréal, 6128 Succursale Centre-Ville, Montréal, QC, Canada H3C 3J7

Edited by Anthony J. Pawson, University of Toronto, Toronto, ON, Canada, and approved December 29, 2007 (received for review October 12, 2007)

RAF kinase functions in the mitogen-activated protein kinase (MAPK) pathway to transmit growth signals to the downstream kinases MEK and ERK. Activation of RAF catalytic activity is facilitated by a regulatory complex comprising the proteins CNK (Connector enhancer of KSR), HYP (Hyphen), and KSR (Kinase Suppressor of Ras). The sterile α -motif (SAM) domain found in both CNK and HYP plays an essential role in complex formation. Here, we have determined the x-ray crystal structure of the SAM domain of CNK in complex with the SAM domain of HYP. The structure reveals a single-junction SAM domain dimer of 1:1 stoichiometry in which the binding mode is a variation of polymeric SAM domain interactions. Through *in vitro* and *in vivo* mutational analyses, we show that the specific mode of dimerization revealed by the crystal structure is essential for RAF signaling and facilitates the recruitment of KSR to form the CNK/HYP/KSR regulatory complex. We present two docking-site models to account for how SAM domain dimerization might influence the formation of a higher-order CNK/HYP/KSR complex.

MAPK signaling | RAF activation | sterile α -motif | x-ray crystallography

The mitogen-activated protein kinase (MAPK) pathways are evolutionarily conserved signal transduction modules of three sequentially activated protein kinases that control cellular growth, differentiation, and survival (reviewed in ref. 1). One such MAPK pathway consists of the cascade through the kinases RAF, MEK, and ERK. The importance of this pathway in regulating growth signals is reflected by the occurrence of mutations in RAF in $\approx 8\%$ of all cancers and $\approx 66\%$ of malignant melanomas (2, 3).

RAF kinases are downstream effectors of the RAS family of small GTPases (reviewed in ref. 4). Although the events leading to RAS activation are now well understood, the precise mechanism by which activated RAS in turn activates RAF to transduce signals to MEK and ERK remains unclear (5). Studies in *Drosophila* S2 cells revealed that activation of RAF kinase at sites of RAS-mediated signaling is facilitated by a regulatory complex comprising the proteins CNK (Connector enhancer of KSR), HYP (Hyphen, also known as Aveugle or AVE), and KSR (Kinase Suppressor of RAS) (6, 7). The sterile α -motif (SAM) domain, present in both CNK and HYP, is essential for the ability of CNK/HYP/KSR to associate and for signals to transduce through the RAF-MEK-ERK cascade (6); see Fig. 1A for schematic of domain architecture.

The structural characterization of SAM domains has revealed the basis by which some SAM domains engage in polymeric protein-protein interactions (8–14), and the basis by which certain SAM domains bind RNA (15–17). A characteristic constellation of basic residues in the sequence of some SAM domains is diagnostic for binding RNA hairpins in a loop sequence-dependent manner (18). In contrast, SAM domains that mediate polymeric protein-protein interactions cannot be readily recognized from their primary sequence alone. Polymer formation by SAM domains in general arises from the interaction of two distinct surfaces on the SAM domain termed the midloop (ML) and end-helix (EH) surfaces (8). Repeating ML/EH interactions of adjacent SAM domains lead to polymer extension.

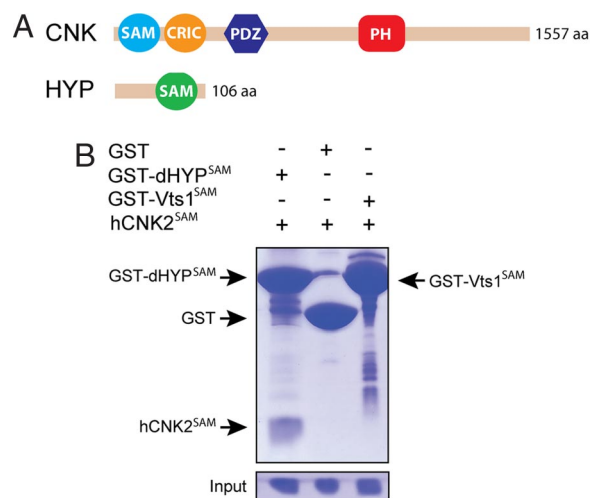


Fig. 1. The SAM domains of CNK and HYP interact directly. (A) Domain architecture of CNK and HYP. CNK is characterized by the presence of a SAM (sterile α -motif) domain; a CRIC (conserved region in CNK); a PDZ (PSD-95, ZO-1/2, Dlg-1) domain; and a PH (pleckstrin homology) domain. HYP contains a single SAM domain. Indicated protein sizes correspond to the *Drosophila* members. (B) Pull-down analysis of GST-dHYP^{SAM} with hCNK2^{SAM}. GST and GST-Vts1^{SAM} served as controls.

SAM domain-mediated polymerization has been shown to underlie many aspects of biological function. For example, SAM domain-mediated polymerization is essential for long-range transcriptional repression by the polycomb group proteins (9). In the TEL transcriptional repressor, which is a common target of chromosomal translocations in several hematological malignancies, the N-terminal SAM domain is frequently fused to various tyrosine kinases that on self-polymerization cause aberrant kinase activation and cell transformation (8). In the yeast MAPK pathway, activation of Ste11 by the scaffold Ste50 appears to involve polymerization through their respective SAM domains (19). This has prompted speculation that perhaps polymerization by the SAM domains of CNK and HYP in metazoan MAPK signaling underlies the for-

Author contributions: T.R. and M.S. contributed equally to this work; T.R., M.S., M. Therrien, and F.S. designed research; T.R., M.S., and I.K. performed research; and T.R., M.S., M. Therrien, and F.S. analyzed data; M. Tyers contributed new reagents/analytic tools; and T.R., M. Therrien, and F.S. wrote the paper.

The authors declare no conflict of interest.

This article is a PNAS Direct Submission.

Data deposition: The atomic coordinates and structure factors have been deposited in the Protein Data Bank, www.pdb.org (PDB ID codes 3B55 and 3B57).

**To whom correspondence may be addressed. E-mail: marc.therrien@umontreal.ca or sicheri@mshri.on.ca.

This article contains supporting information online at www.pnas.org/cgi/content/full/0709705105/DC1.

© 2008 by The National Academy of Sciences of the USA

mation of a large signaling complex that recruits an activator of RAF (7).

In this report, we show that the CNK/HYP interaction is in fact mediated directly by their SAM domains. However, by using x-ray crystallography, we demonstrate that the SAM domain of CNK forms a finite (discrete) heterodimer with the SAM domain of HYP. This interaction occurs through a ML/EH binding mode that is very similar to that seen in polymeric SAM interactions. A 1:1 binding stoichiometry results from the presence of only a single interaction surface on the CNK and HYP SAM domains. We show that SAM domain-mediated dimerization of CNK/HYP is essential for RAF signaling *in vivo*. Furthermore, we show that CNK/HYP dimerization is necessary to recruit KSR to form a CNK/HYP/KSR complex through a direct interaction with the kinase domain of KSR. This suggests that, in addition to merely acting as a passive protein-protein interaction module, SAM domains can also function as molecular switches to regulate further signaling events. The CNK/HYP SAM domain complex structure adds to the versatility in binding modes exemplified by this abundant protein domain.

Results

The SAM Domains of CNK and HYP Form a Stable Complex. To determine whether the SAM domains of CNK and HYP interact directly and independently of other factors, we expressed minimal SAM domain constructs in bacteria and tested for an interaction by using an *in vitro* pull-down assay. We screened for suitable expression constructs for the SAM domains of CNK and HYP from different species including *Drosophila*, mouse, and human. We successfully identified expression constructs for the SAM domains of human CNK2 (hCNK2^{SAM}) and *Drosophila* HYP (dHYP^{SAM}). By using a GST pull-down assay, we found that GST-dHYP^{SAM} bound to hCNK2^{SAM} (Fig. 1B). In contrast, GST protein alone or the RNA binding SAM domain of Vts1 fused to GST did not bind to hCNK2^{SAM}. Because SAM domain interactions are known to form multiple oligomeric states, we performed size exclusion chromatography experiments to estimate the stoichiometry of the overall hCNK2^{SAM}/dHYP^{SAM} complex. Separately, purified hCNK2^{SAM} and dHYP^{SAM} elute as monomers, whereas a copurified hCNK2^{SAM}/dHYP^{SAM} complex elutes with an apparent molecular mass consistent with a dimeric complex [see [supporting information \(SI Fig. 5\)](#)]. To determine the dissociation constant for dimerization, we used surface plasmon resonance experiments and found that the K_d for dimerization is 92.5 nM (SI Fig. 6). Taken together, these results indicate that hCNK2^{SAM} binds tightly and directly *in vitro* with an apparent 1:1 stoichiometry to the dHYP SAM domain.

Structure of the hCNK2^{SAM}/dHYP^{SAM} Complex. Because the ML/EH binding mode is characteristic of polymeric SAM domains, we questioned whether the discrete dimerization of hCNK2^{SAM}/dHYP^{SAM} involves a novel binding mode or a variation of the polymerization binding mode. To distinguish between these two possibilities, we solved the structure of the hCNK2^{SAM}/dHYP^{SAM} complex by x-ray crystallography. Crystals containing a single copy of the complex in the asymmetric unit, belonging to the space group $P2_12_12_1$, were obtained and the structure was solved by using the selenomethionine single-wavelength anomalous dispersion (SAD) phasing method. The final model was refined to 2.0-Å resolution to an $R_{\text{factor}}/R_{\text{free}}$ of 21.4%/24.0%. We also obtained crystals of the isolated dHYP^{SAM} containing two monomers in the asymmetric unit belonging to the space group $C222_1$. The isolated dHYP^{SAM} structure was solved by molecular replacement by using the dHYP^{SAM} structure from the hCNK2^{SAM}/dHYP^{SAM} complex as a search model. The final isolated dHYP^{SAM} structure was refined at 1.9-Å resolution to an $R_{\text{factor}}/R_{\text{free}}$ of 21.7%/26.5%. Pertinent structure determination and refinement statistics are presented in SI Table 1.

Both hCNK2^{SAM} and dHYP^{SAM} adopt the canonical five helix

($\alpha 1$ - $\alpha 5$) SAM domain fold in complex (Fig. 24). The structure of dHYP^{SAM} bound to hCNK2^{SAM} is virtually unchanged from the isolated dHYP^{SAM} structure with a rms deviation of 0.4 Å for 74 C α atoms (SI Fig. 7). The structure of the complex reveals heterodimerization to be a variation of the polymer theme in which the EH surface of hCNK2^{SAM} engages the ML surface of dHYP^{SAM} (Fig. 2B). The hCNK2^{SAM}/dHYP^{SAM} interface buries ≈ 580 Å² of surface area on each SAM domain and involves a higher proportion of polar contacts than observed previously in other ML/EH SAM domain complexes (8–14). The ML surface of dHYP^{SAM} is partly comprised by Asp-53, Arg-57, Arg-61, and Arg-69. These charged residues engage in multiple salt-bridge interactions with the oppositely charged side chains of Asp-24, Glu-53, His-62, Glu-64, Glu-68, and Asp-71 on the EH surface of hCNK2^{SAM} (Fig. 2B). Hydrophobic dimer contacts are formed by Ile-54, Ala-58, and Ile-62 on the ML surface of dHYP^{SAM} and by Ile-60, Gly-61, and Leu-65 on the EH surface of hCNK2^{SAM}. The small side chain of Gly-61 allows hCNK2^{SAM} helix $\alpha 5$ to pack tightly against the ML surface of dHYP^{SAM}.

Consistent with the finding that the hCNK2^{SAM}/dHYP^{SAM} complex is a discrete dimer and not a polymer, only one of the two polymerizing surfaces on each SAM domain is highly conserved. Specifically, the EH surface on hCNK2^{SAM} orthologues and the ML surface on dHYP^{SAM} orthologues show striking conservation (Fig. 3). Notably, the ML surface of hCNK2^{SAM} and the EH surface of dHYP^{SAM} are not conserved in orthologous proteins. This contrasts sharply with the polymerizing SAM domain of Polyhomeotic (Ph^{SAM}) for which both the ML and EH surfaces are conserved (Fig. 3). The inability of hCNK2^{SAM} and dHYP^{SAM} to interact by their ML and EH surfaces, respectively, would explain why the two proteins form discrete dimers rather than extended polymers.

Validation of the hCNK2^{SAM}/dHYP^{SAM} Dimer Interface: *In Vitro*. To identify the essential determinants of dimerization and to confirm that the crystal structure reflects the solution structure of the hCNK2^{SAM}/dHYP^{SAM} complex, we individually substituted surface contact residues on hCNK2^{SAM} and dHYP^{SAM} and analyzed the interaction potential of these mutants by using a GST pull-down assay (Fig. 4A and B). In agreement with predictions from the crystal structure, a R61E charge reversal mutation on the ML surface of dHYP^{SAM} strongly reduced binding to hCNK2^{SAM} (Fig. 4A). Introduction of a double-charge reversal R57E/R61E at the ML surface resulted in no detectable interaction with hCNK2^{SAM}. In contrast, a R57A/R61A double mutant showed only a reduced ability to interact.

In converse experiments, a R59S/E68G double mutation or the D71A single mutation on the EH surface of hCNK2^{SAM} had no effect on the capacity to interact with GST-dHYP^{SAM} (Fig. 4B). The D71R and I60A single mutants of the EH surface showed a modestly reduced ability to bind GST-dHYP^{SAM}. The double-charge reversal E68R/D71R at the EH surface resulted in no detectable interaction with GST-dHYP^{SAM}. A control mutation Y78A outside the EH surface on hCNK2^{SAM} had no effect on binding to GST-dHYP^{SAM}. These results confirm that the x-ray structure reflects the solution interaction of hCNK2^{SAM}/dHYP^{SAM}.

The observation that different mutants had different effects on the ability to dimerize can be reconciled by the crystal structure. The R57E/R61E dHYP^{SAM} double mutant likely destabilizes the SAM/SAM complex most by abrogating four favorable salt-bridge interactions and introducing a strong electrostatic repulsion at the interface (Fig. 2B). The single R61E dHYP^{SAM} mutant perturbs only two salt-bridge interactions and introduces a weaker electrostatic repulsion than with the R57E/R61E dHYP^{SAM} mutant, thus disrupting the interaction to a lesser extent (Fig. 4A). The R57A/R61A dHYP^{SAM} mutant perturbs four salt-bridge interactions, but does not introduce any electrostatic repulsion at the interface. Hence, the R57A/R61A mutant shows the least effect on perturbing dimerization relative to the charge reversal mutations. A similar

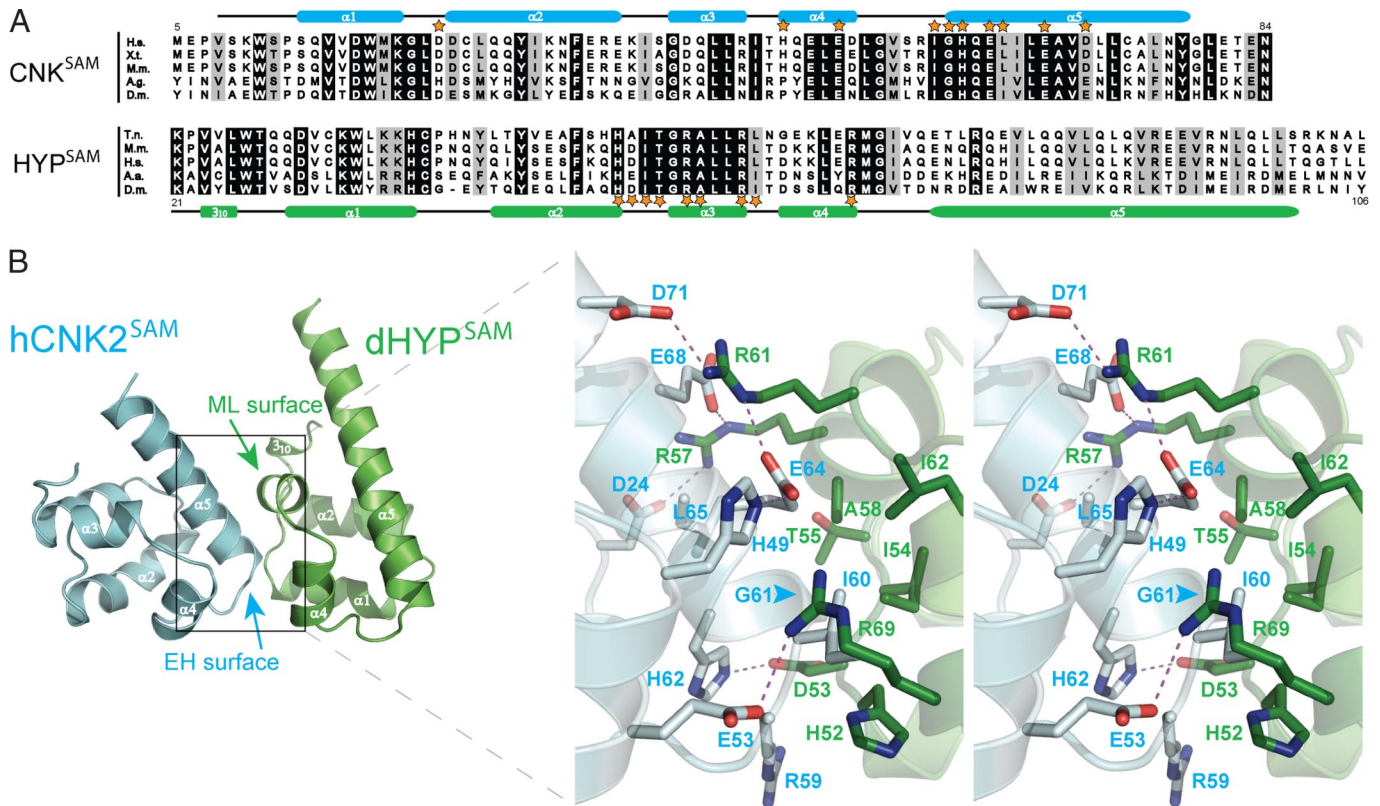


Fig. 2. The EH surface of hCNK2^{SAM} recognizes the ML surface of dHYP^{SAM}. (A) CNK^{SAM} and HYP^{SAM} sequence alignments are shown with invariant positions indicated in black, or positions showing conservation of certain residue properties (e.g., charge, hydrophobicity) in gray. Secondary structures of hCNK2^{SAM} and dHYP^{SAM} are indicated with helices in cyan and green cylinders, respectively. Interface residues of hCNK2^{SAM} and dHYP^{SAM} are indicated by orange stars. A.a., *Aedes aegypti*; A.g., *Anopheles gambiae*; H.s., *Homo sapiens*; M.m., *Mus musculus*; T.n., *Tetraodon nigroviridis*; X.t., *Xenopus tropicalis*. (B) Stereoview of dimer interface. Salt-bridge interactions are highlighted by dashed lines.

rationale explains the more potent effect on dimerization caused by the D71R charge reversal mutant of hCNK2^{SAM} versus the D71A mutant (Fig. 4B).

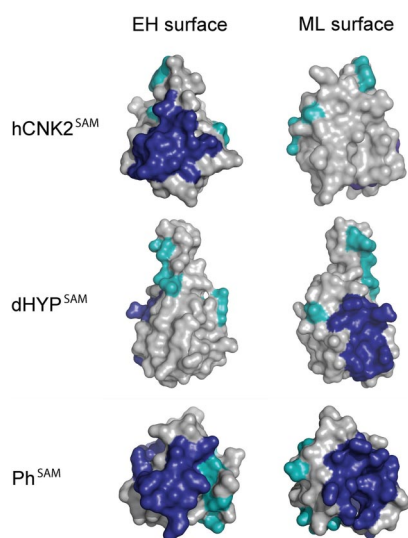


Fig. 3. Surface mapping of conserved residues on CNK^{SAM}, HYP^{SAM}, and Ph^{SAM}. Conservation based on sequence alignments of orthologues from the six species indicated in Fig. 2A. Conserved residues with >50% solvent-exposed side chains are colored such that those at the ML/EH surfaces are shown in blue, and all others are shown in teal.

Validation of the hCNK2^{SAM}/dHYP^{SAM} Dimer Interface: *In Vivo*. We next sought verification that the cross-species complex between hCNK2^{SAM} and dHYP^{SAM} in the crystal structure and in solution reflects the homo-species complex formed by dCNK/dHYP *in vivo*. For this, we prepared a series of mutants that targeted SAM domain dimer interface surface residues on dHYP and dCNK constructs. For dCNK, we used a construct that included the SAM-CRICK-PDZ regions (denoted dCNK²⁻⁵⁴⁹; see Fig. 1A), because the SAM domain alone or a SAM-CRICK construct were not detectably expressed in S2 cells. We then introduced mutations of interface residues equivalent to those on the EH surface of hCNK2^{SAM} in dCNK²⁻⁵⁴⁹. The mutant constructs were transfected into S2 cells and the overexpressed proteins were tested for binding in a GST pull-down assay (Fig. 4C). Although wild-type dHYP bound strongly to wild-type dCNK²⁻⁵⁴⁹, the single mutation R61D and the double mutation R57A/R61A on dHYP severely reduced binding to wild type dCNK²⁻⁵⁴⁹ (Fig. 4C). The double-charge reversal mutation R57D/R61D on dHYP caused the strongest reduction on the interaction with dCNK²⁻⁵⁴⁹, consistent with the strongest effect seen for the double-charge reversal in the *in vitro* pull-down assay (Fig. 4A).

On the EH surface of dCNK²⁻⁵⁴⁹, the double mutation R57S/E66G and the single mutation E69A each showed a minor effect on the ability to interact with dHYP (Fig. 4D). The single mutations E69R and I58A each showed a moderately reduced capacity to interact with dHYP, whereas the double-charge reversal E66R/E69R on the EH surface of dCNK²⁻⁵⁴⁹ showed a complete loss of binding, paralleling the effects seen *in vitro*. The control mutation Y76A on dCNK²⁻⁵⁴⁹ on a surface outside the dimer interface had no effect on binding. These results confirm that the dimer interface

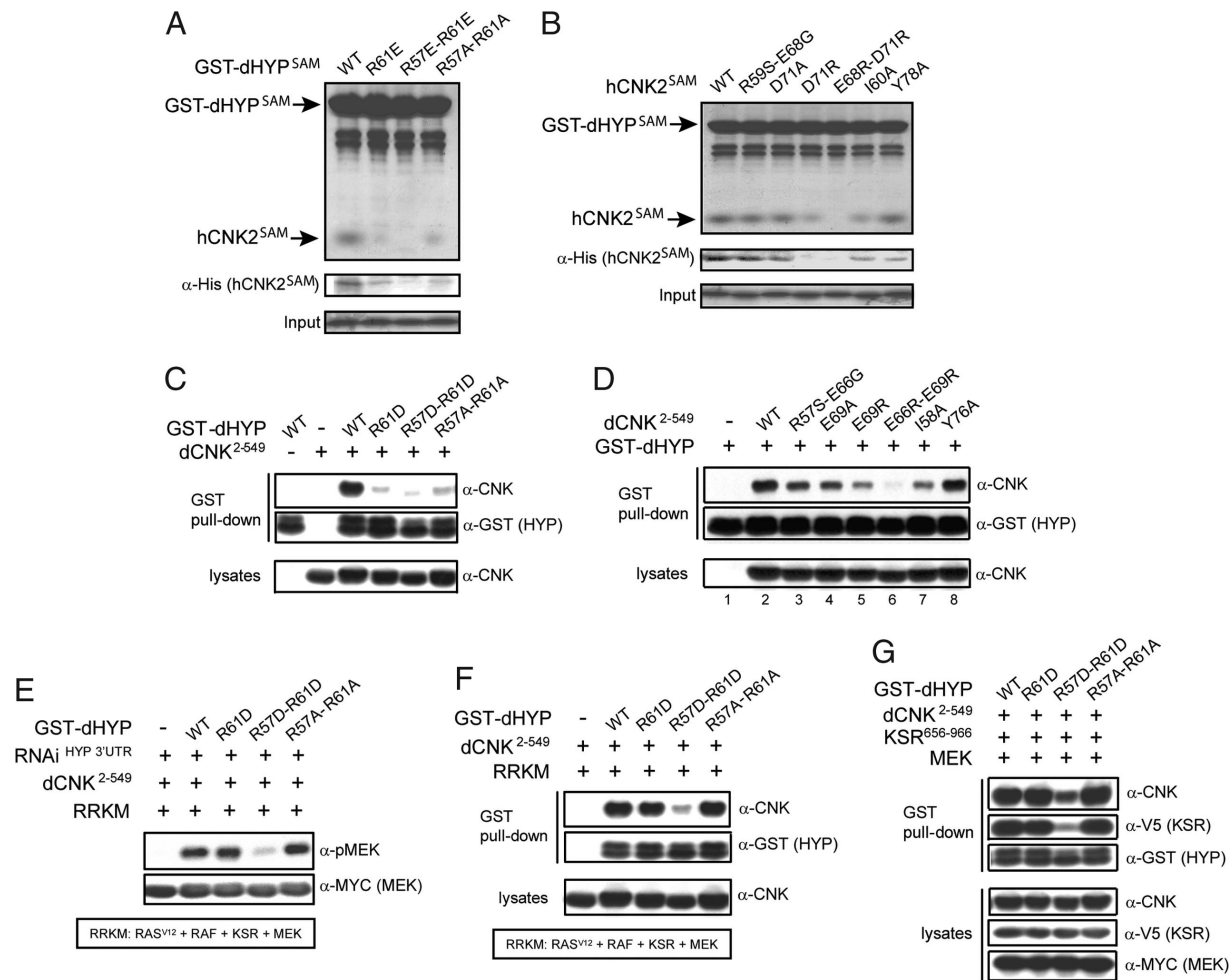


Fig. 4. CNK/HYP SAM domain complex regulates RAF signaling by recruiting KSR. (A and B) GST pull-down assay of wild-type or dimer interface mutant variants of GST-dHYP^{SAM} or hCNK2^{SAM}. The Y78A mutation outside the EH surface on hCNK2^{SAM} served as a control. (C and D) GST pull-down assay from S2 cell co-overexpressing wild-type or dimer interface mutants of GST-dHYP or dCNK²⁻⁵⁴⁹. The Y76A substitution served as a control. Equal expression of GST-dHYP and dCNK²⁻⁵⁴⁹ proteins were confirmed by αGST and αCNK blotting of the primary lysates, respectively. (E) dHYP dimer interface mutants were tested for their ability to stimulate RAF activity as measured by MEK phosphorylation (pMEK) levels. (F) GST pull-down assays were performed as in Fig. 4C, except S2 cells were cotransfected with wild-type dCNK²⁻⁵⁴⁹, wild-type, or indicated GST-dHYP mutants, Ras^{V12}, RAF, KSR, and MEK. (G) Similar GST-pull downs as in Fig. 4F were repeated in the presence of wild-type dCNK²⁻⁵⁴⁹, KSR kinase domain and MEK along with wild type or the indicated GST-dHYP mutants. Equal expression of proteins was confirmed by blotting of the primary lysates.

revealed by the crystal structure of hCNK2^{SAM}/dHYP^{SAM} reflects the interaction of dCNK²⁻⁵⁴⁹/dHYP *in vivo*.

CNK/HYP Dimerization Is Essential for RAF Signaling *in Vivo*. We next tested the relevance of the CNK/HYP SAM domain interaction for RAF activation downstream of a dominant active mutant of RAS (Ras^{V12}) in S2 cells. In this assay, the co-overexpression of Ras^{V12}, RAF, KSR, and MEK is sufficient to reconstitute RAF signaling in a dCNK²⁻⁵⁴⁹- and dHYP-dependent manner. Activation of RAF kinase results in phosphorylation of its substrate MEK that can be detected by immunoblotting with an anti-phospho-MEK antibody. Using RNAi, we depleted endogenous dHYP and found that this abolishes MEK phosphorylation as reported (6) (Fig. 4E; SI Fig. 8). We then introduced RNAi-insensitive variants of wild-type or dimerization-defective dHYP constructs and tested for their ability to restore RAF kinase activity as indicated by phospho-MEK levels. Although wild-type dHYP restored MEK phosphorylation, the R57D/R61D dHYP mutant failed to restore phospho-MEK levels, indicating that a direct dCNK^{SAM}/dHYP^{SAM} interaction is essential for RAF signaling. Surprisingly, the R61D and R57A/R61A dHYP mutants fully restore phospho-MEK levels to that of wild-type dHYP, despite their reduced binding to dCNK²⁻⁵⁴⁹ in the previous

pull-down assay (Fig. 4C). These results indicate that, although the R61D and R57A/R61A dHYP mutants are both impaired in their capacity to bind dCNK²⁻⁵⁴⁹, only the stronger R57D/R61D dHYP mutant shows both impaired binding and RAF-signaling defects.

A CNK/HYP Complex Recruits KSR. The reduced interaction of the R61D and R57A/R61A dHYP mutants with dCNK²⁻⁵⁴⁹ contrasts with the apparently normal function of these mutants in RAF signaling *in vivo*. We reasoned that this apparent contradiction could be attributed to CNK and HYP acting within a larger protein complex. In this context, secondary interactions outside of the SAM domain are sufficient to stabilize protein complex formation in the case of weakly perturbing SAM/SAM mutations. One simple explanation then for the outwardly normal restoration of phospho-MEK levels in our RAF-signaling assay by R61D and R57A/R61A dHYP mutants is that the co-overexpression of other signaling components in the assay, such as Ras^{V12}, RAF, KSR, and MEK, offsets the weaker dimerization defect of R61D and R57A/R61A dHYP mutants.

To characterize the component(s) that may be compensating for the R61D and R57A/R61A dHYP mutations, we first determined whether the co-overexpression of Ras^{V12}, RAF,

KSR, and MEK as in our RAF-signaling assay could restore the binding of R61D and R57A/R61A dHYP mutants to dCNK²⁻⁵⁴⁹ in the GST pull-down assay. As shown in Fig. 4F, this is indeed what we observed because the R61D and R57A/R61A dHYP mutants associate with dCNK²⁻⁵⁴⁹ as efficiently as wild-type dHYP when co-overexpressed with Ras^{V12}, RAF, KSR, and MEK. In contrast, the R57D/R61D dHYP mutant is still defective in binding to dCNK²⁻⁵⁴⁹.

Next, we attempted to identify which of Ras^{V12}, RAF, KSR, and MEK contribute to the restored binding of R61D and R57A/R61A dHYP mutants to dCNK²⁻⁵⁴⁹. Because the function of CNK in promoting RAF activation was previously shown to depend on determinants within the kinase domain of KSR (6), we hypothesized that the kinase domain of KSR might compensate for the dimerization defect of R61D and R57A/R61A dHYP mutants. To test this, we co-overexpressed KSR kinase domain along with dHYP and dCNK²⁻⁵⁴⁹ to test for binding in our GST pull-down assay (MEK was also coexpressed with KSR kinase domain because overexpressed KSR kinase domain alone is unstable in the absence of co-overexpressed MEK). As shown in Fig. 4G, under these conditions, the R61D and R57A/R61A dHYP mutants associate with dCNK²⁻⁵⁴⁹ as stably as wild-type dHYP, even though these mutants showed a significantly reduced binding to dCNK²⁻⁵⁴⁹ in the absence of co-overexpressed KSR kinase domain (Fig. 4C). In contrast, the R57D/R61D dHYP mutant is still severely impaired in binding to dCNK²⁻⁵⁴⁹. These results are consistent with our RAF-signaling results and identify KSR as part of the dCNK²⁻⁵⁴⁹/dHYP complex that stabilizes the SAM-SAM interaction. Moreover, the pull-down assays localize the minimal region of KSR required for this effect to be the protein kinase domain (Fig. 4G). Taken together, our results suggest that the dimerization of CNK and HYP mediated by their SAM domains facilitates KSR recruitment through the kinase domain of KSR to form the CNK/HYP/KSR complex.

Models for KSR Binding to CNK/HYP. The compromised interaction of the kinase domain of KSR in the context of the R57D/R61D dHYP mutant suggests that the SAM/SAM complex of CNK/HYP might form a composite docking site for KSR binding. We reasoned that if such a site existed, we might be able to identify it on the basis of sequence conservation as seen for the ML/EH surfaces. By mapping conserved surface residues on the hCNK^{2SAM}/dHYP^{SAM} complex, we identified a candidate interaction site encompassing the C termini of helix $\alpha 5$ in both CNK and HYP SAM domains. This region of each SAM domain is solvent-exposed, reasonably well conserved, and spatially juxtaposed (SI Fig. 9A). Consistent with the possibility that this region constitutes an interaction site for the kinase domain of KSR as modeled in SI Fig. 9B, we found that a triple mutation D81A/N82A/L83A in CNK targeting three conserved residues just outside the last ordered residue seen in our crystal structure selectively perturbs the interaction with KSR, but not with HYP (data not shown).

Our ability to test this composite binding site model was hampered by protein expression issues. Specifically, we cannot express the isolated SAM domains of dCNK or hHYP or the kinase domain of hKSR, which would allow us to test for direct binding of proteins from a common species. We found that a minimal SAM domain dimer between hCNK2 and dHYP does not bind to the kinase domain of dKSR, but that this was likely due to a cross-species effect (SI Fig. 10A and B). Indeed, whereas a single-species complex between dCNK²⁻⁵⁴⁹/dHYP binds to the kinase domain of dKSR, the equivalent cross-species complex of hCNK²⁻⁴⁸⁵/dHYP does not (SI Fig. 10B). As such, a second KSR binding model that cannot be ruled out at this time is one in which the CRIC-PDZ region C-terminal to the SAM domain in CNK constitutes the KSR kinase domain binding site. Presumably, this site remains hidden until the SAM domain of HYP engages the SAM domain of CNK (SI Fig. 9C).

Discussion

CNK/HYP/KSR Complex Is Required for RAF Signaling. Building on previous biochemical studies, our results present a structural link between CNK, HYP, and KSR in RAS-induced RAF activation. We find that SAM domains mediate direct interaction between CNK and HYP. The CNK^{SAM}/HYP^{SAM} complex forms a discrete ML/EH surface dimer incapable of polymerization. We show that this dimerization event is required to recruit KSR to form a CNK/HYP/KSR regulatory complex necessary for signaling through the RAF-MEK-ERK module.

The formation of the CNK/HYP/KSR complex involves minimally the SAM domains of CNK/HYP and the kinase domain of KSR. It is worth noting that, although we coexpressed KSR with MEK in our *in vivo* assays and this raises the possibility that MEK bridges the CNK/HYP/KSR interaction, this scenario is unlikely. First, previous studies showed that endogenous CNK/HYP/KSR complex formation is unperturbed in the presence of RNAi knock-down of endogenous MEK in S2 cells, but complex formation is compromised by RNAi against endogenous CNK, HYP, or KSR (6). Second, KSR mutants unable to interact with MEK still retain their capacity to bind CNK/HYP (data not shown). Thus, we reason that in the context of our overexpressed pull-down assays, MEK serves only to improve expression of the kinase domain of KSR.

Structural Basis for Discrete SAM Domain Interactions. Our structural characterization of the hCNK^{2SAM}/dHYP^{SAM} complex provides the first high-resolution view of a discrete SAM/SAM complex and reveals that discrete SAM domain dimerization can also occur through the ML and EH surfaces previously known to mediate polymerization. The ML surface on HYP^{SAM} has evolved to selectively recognize the EH surface on CNK^{SAM} with high affinity. In contrast, the EH and ML surfaces on HYP^{SAM} and CNK^{SAM}, respectively, are nonfunctional and show no sequence conservation across species. We presume that there has been no selective pressure for maintaining residues at the nonfunctional surfaces.

We reason that discrete dimerization of SAM domains, as seen for the hCNK^{2SAM}/dHYP^{SAM} interaction, might have relevance for other SAM domain interactions in addition to the more common polymeric interactions that have been reported (8–14). Indeed, a recent study has identified the SAM domain complex of Arap3/SHIP2 that forms discrete dimers in solution (20). Whether the Arap3/SHIP2 mode of dimerization also involves ML/EH surfaces is unknown. Regardless, the involvement of the ML/EH surfaces in other discrete SAM domain interactions is also suggested from a mutational analysis on the SAM domain interaction of Byr2 and Ste4 in which residues at the putative ML and EH surfaces, respectively, were found to contribute to the formation of finite oligomers (21).

Conclusion

The dysregulation of RAF and its upstream regulator RAS in many human tumors and the drugability of protein kinases in general has identified RAF as an attractive target for therapeutic intervention (22). Because RAF activation depends on the action of the CNK/HYP/KSR complex, this complex too might provide targets for intervention in this regard. Our work identifies specific interactions that are essential for RAF activity and may in the future be amenable to modulation by small molecule inhibitors.

Materials and Methods

Plasmids. The SAM domain of human CNK2 (residues 5–84) was amplified by PCR and subcloned into the pProEx-HTa expression vector (Invitrogen). Full-length dHYP and the minimal SAM domain construct (residues 21–98) were PCR-amplified and inserted into the pETM-30 vector (EMBL, Protein Expression Facility). Variant SAM domain mutants were generated by two-step PCR-based targeted mutagenesis.

Copper-inducible pMet vectors were used for binding and functional assays conducted in S2 cells (23). pMet-HA-RAS^{V12}, pMet-MYC-MEK, pMet-PYO-RAF,

pMet-V5-KSR, pMet-PYO-HYP, HYP dsRNAs, and pMet-FLAG-dCNK²⁻⁵⁴⁹ have been described (6, 24). pMet-GST-HYP was generated in two steps. First, a GST cDNA (pGEX4T; Amersham Biosciences) containing a 6xHis tag and a TEV cleavage site at its C terminus was amplified by PCR and introduced in pMet vector. Second, a *Drosophila* Hyphen cDNA (residues 2–106) was amplified by PCR and introduced at the C terminus of GST-His-TEV to create pMet-GST-HYP. Variant HYP and CNK mutants were generated by using the QuikChange procedure (Clontech).

Protein Expression and Purification. Proteins were expressed in *Escherichia coli* BL21 (DE3) strain (Novagen). Proteins were purified by Ni affinity chromatography by using a HiTrap Chelating HP column (Amersham) and eluted with imidazole. The eluate was treated with TEV to cleave off the 6xHis tag in pProEx-HTa or the 6xHis-GST tag in pETM-30. TEV-cleaved proteins were dialyzed into buffer and applied to a HiTrap Chelating HP column to elute untagged proteins. Eluate was concentrated and applied to a Superdex 75 gel filtration column (Amersham) for final purification. To obtain a selenomethionyl derivative of hCNK2^{SAM} and dHYP^{SAM}, *E. coli* B834 cells were transformed and grown in minimal medium supplemented with selenomethionine. All proteins were purified into buffer containing 10 mM Hepes (pH 7.0), 200 mM NaCl, and 5 mM β -mercaptoethanol.

Crystallization, Data Collection, Structure Determination, and Modeling. Crystals were grown by the hanging-drop vapor diffusion method. hCNK2^{SAM}/dHYP^{SAM} cocrystals were grown at 4°C by mixing 1 μ l of 4–8 mg·ml⁻¹ of each protein with 1 μ l of well buffer (100 mM Tris, pH 7.0–7.5, and 12–18% PEG 2000 MME). Flash-freezing of the crystals was performed by using the crystallization buffer supplemented with 25% (vol/vol) glycerol. Data were collected at the Advanced Photon Source (APS) of the Argonne National Laboratory on Beamline 24-ID of NE-CAT and analyzed by using the HKL2000 software package (25). The SHELX (26) set of programs was used to locate heavy-atom sites, calculate phases, and perform density modification. Electron density maps calculated from the phases after density modification were used to build an initial model in ARP/wARP (27) and refined by using REFMAC5 (28) in the CCP4 software package. A representative $|2F_o - F_c|$ map of the hCNK2^{SAM}/dHYP^{SAM} complex is shown in **SI Fig. 11**.

dHYP^{SAM} alone crystals were grown at 20°C by mixing 1 μ l of 13 mg·ml⁻¹ protein with 1 μ l of well buffer (100 mM cacodylate, pH 6.5, and 1 M sodium citrate). Flash-freezing of the crystals was performed by using the crystallization buffer supplemented with 25% (vol/vol) glycerol. Data were collected under a liquid nitrogen stream at the APS on Beamline 14-BM-C of BioCARS and analyzed by using the HKL2000 software package (25). The program PHASER (29) in the CCP4 package was used to find a molecular replacement solution based on the dHYP^{SAM} structure of the hCNK2^{SAM}/dHYP^{SAM} complex as the search model. REFMAC5 (28) was used for iterative cycles of refinement in between manual

refinement by using Coot (30). Ribbons and surface representations were generated by using PyMOL (DeLano Scientific).

Surface Plasmon Resonance Experiments. Surface plasmon resonance experiments for the hCNK2^{SAM}/dHYP^{SAM} interaction were performed at room temperature in 10 mM Hepes, pH 7.0, and 200 mM NaCl. dHYP^{SAM} was immobilized on a Biacore Pioneer CM5 sensor chip (GE Healthcare) according to the manufacturer's instructions. Free hCNK2^{SAM} protein was injected and the binding data were analyzed by using BIAevaluation 3.0 software.

GST Pull-Down Assays. A 30- μ l sample of 50% slurry of glutathione Sepharose 4B beads (Amersham Pharmacia) was equilibrated in assay buffer (10 mM Hepes, pH 7.0, 100 mM NaCl, and 10 mM β -mercaptoethanol). The slurry was mixed with 30 μ l of \approx 4 mg·ml⁻¹ GST-fusion protein and incubated for 15 min at 4°C on a nutator. The beads were washed three times with 1 ml of the assay buffer and then nutated with 30 μ l of 4 mg·ml⁻¹ of 6xHis-tagged protein in a final volume of a 500- μ l assay buffer for 1 h at 4°C. The beads were subjected to three washes with 1 ml of the assay buffer. SDS loading buffer was added to the samples and heated at 90°C for 10 min. Proteins were resolved on precast 4–20% (Invitrogen) SDS/PAGE and visualized by Coomassie blue staining. Identical samples were resolved by 17% SDS/PAGE and subjected to immunoblot analysis by using antibodies specific for the 6xHis tag (Sigma).

S2 Cell Assays. S2 cells were grown in serum-free insect cell medium (Sigma). Transfection and induction of protein expression were conducted as described in ref. 24. At 36 h postinduction cells were lysed in Nonidet P-40 lysis buffer (20 mM Tris, pH 8.0, 137 mM NaCl, 1% Nonidet P-40, 10% glycerol, and 1 mM EDTA).

For GST pull-down assays, 50 μ l of 50% slurry of glutathione Sepharose 4B beads (GE Healthcare) equilibrated in lysis buffer was added to protein lysates and rocked for 4 h at 4°C. Beads were then washed three times with 1 ml of lysis buffer and proteins were eluted with 50 μ l of elution buffer (5 mM L-glutathione, 50 mM Tris, pH 8.0).

Total protein lysates or eluted proteins were resolved on 8–10% SDS/PAGE, transferred to nitrocellulose membranes and immuno-detected by using either rabbit α -GST (Calbiochem), mouse α -V5 (Invitrogen), rabbit α -pMEK (Cell Signaling), or mouse antibodies α -CNK, α -MYC, α -PYO, and α -HA as described in ref. 31.

ACKNOWLEDGMENTS. We thank BioCARS and NE-CAT, Advanced Photon Source, Argonne, IL, for access to the 14-MB-C and 24-ID beamlines, respectively, and the members of the Sicheri laboratory for helpful discussions. This work was supported by grants from the Canadian Institutes for Health Research (to F.S. and M.T.) and by a grant from the National Cancer Institute of Canada with funds from the Cancer Research Society (to M.T.). T.R. is a recipient of a University of Toronto Open Fellowship, M.T. is a Canada Research Chair (Tier II) in Intracellular Signaling, and F.S. is a recipient of a National Cancer Institute of Canada Scientist award.

- Kolch W (2005) Coordinating ERK/MAPK signalling through scaffolds and inhibitors. *Nat Rev Mol Cell Biol* 6:827–837.
- Rushworth L-K, Hindley A-D, O'Neill E, Kolch W (2006) Regulation and role of Raf-1/B-Raf heterodimerization. *Mol Cell Biol* 26:2262–2272.
- Mercer K, et al. (2005) Expression of endogenous oncogenic V600E-raf induces proliferation and developmental defects in mice and transformation of primary fibroblasts. *Cancer Res* 65:11493–11500.
- Wellbrock C, Karasarides M, Marais R (2004) The RAF proteins take centre stage. *Nat Rev Mol Cell Biol* 5:875–885.
- Claperton A, Therrien M (2007) KSR and CNK: Two scaffolds regulating RAS-mediated RAF activation. *Oncogene* 26:3143–3158.
- Douziech M, Sahmi M, Laberge G, Therrien M (2006) A KSR/CNK complex mediated by HYP, a novel SAM domain-containing protein, regulates RAS-dependent RAF activation in *Drosophila*. *Genes Dev* 20:807–819.
- Roignant J-Y, Hamel S, Janody F, Treisman J-E (2006) The novel SAM domain protein Aveugle is required for Raf activation in the *Drosophila* EGF receptor signaling pathway. *Genes Dev* 20:795–806.
- Kim C-A, et al. (2001) Polymerization of the SAM domain of TEL in leukemogenesis and transcriptional repression. *EMBO J* 20:4173–4182.
- Kim C-A, Gingery M, Pilpa R-M, Bowie J-U (2002) The SAM domain of polyhomeotic forms a helical polymer. *Nat Struct Mol Biol* 9:453–457.
- Tran H-H, Kim C-A, Faham S, Siddall M-C, Bowie J-U (2002) Native interface of the SAM domain polymer of TEL. *BMC Struct Biol* 2:5.
- Kwan J-J, Warner N, Pawson T, Donaldson L-W (2004) The solution structure of the *S. cerevisiae* Ste11 MAPKKK SAM domain and its partnership with Ste50. *J Mol Biol* 342:681–693.
- Qiao F, et al. (2004) Derepression by depolymerization; structural insights into the regulation of Yan by Mae. *Cell* 118:163–173.
- Kim C-A, Sawaya M-R, Cascio D, Kim W, Bowie J-U (2005) Structural organization of a Sex-comb-on-midleg/polyhomeotic copolymer. *J Biol Chem* 280:27769–27775.
- Baron M-K, et al. (2006) An architectural framework that may lie at the core of the postsynaptic density. *Science* 311:531–535.
- Aviv T, Lin Z, Ben-Ari G, Smibert C-A, Sicheri F (2006) Sequence-specific recognition of RNA hairpins by the SAM domain of Vts1p. *Nat Struct Mol Biol* 13:168–176.
- Johnson P-E, Donaldson L-W (2006) RNA recognition by the Vts1p SAM domain. *Nat Struct Mol Biol* 13:177–178.
- Oberstrass F-C, et al. (2006) Shape-specific recognition in the structure of the Vts1p SAM domain with RNA. *Nat Struct Mol Biol* 13:160–167.
- Green J-B, Gardner C-D, Wharton R-P, Aggarwal A-K (2003) RNA recognition via the SAM domain of Smaug. *Mol Cell* 11:1537–1548.
- Bhattacharjya S, Xu P, Chakrapani M, Johnston L, Ni F (2005) Polymerization of the SAM domain of MAPKKK Ste11 from the budding yeast: Implications for efficient signaling through the MAPK cascades. *Protein Sci* 14:828–835.
- Raaijmakers J-H, et al. (2007) The PI3K effector Arp3 interacts with the PI (3,4,5)P3 phosphatase SHIP2 in a SAM domain-dependent manner. *Cell Signal* 19:1249–1257.
- Ramachander R, Bowie J-U (2004) SAM domains can utilize similar surfaces for the formation of polymers and closed oligomers. *J Mol Biol* 342:1353–1358.
- Li N, Batt D, Warmuth M (2007) B-Raf kinase inhibitors for cancer treatment. *Curr Opin Investig Drugs* 8:452–456.
- Therrien M, Wong A-M, Rubin G-M (1998) CNK, a RAF-binding multidomain protein required for RAS signaling. *Cell* 95:343–353.
- Roy F, Laberge G, Douziech M, Ferland-McCollough D, Therrien M (2002) KSR is a scaffold required for activation of the ERK/MAPK module. *Genes Dev* 16:427–438.
- Otwiniowski Z, Minor W (1997) Processing of x-ray diffraction data collected in oscillation mode. *Methods Enzymol* 276:307–326.
- Sheldrick G-M, Schneider T-R (1997) SHELXL: High-resolution refinement. *Methods Enzymol* 277:319–343.
- Morris R-J, Perrakis A, Lamzin V-S (2002) ARP/wARP's model-building algorithms. I. The main chain. *Acta Crystallogr D Biol Crystallogr* 58:968–975.
- Murshudov G-N, Vagin A-A, Dodson E-J (1997) Refinement of macromolecular structures by the maximum-likelihood method. *Acta Crystallogr D Biol Crystallogr* 53:240–255.
- McCoy A-J, Grosse-Kunstleve R-W, Storoni L-C, Read R-J (2005) Likelihood-enhanced fast translation functions. *Acta Crystallogr D Biol Crystallogr* 61:458–464.
- Emsley P, Cowtan K (2004) Coot: Model-building tools for molecular graphics. *Acta Crystallogr D Biol Crystallogr* 60:2126–2132.
- Douziech M, et al. (2003) Bimodal regulation of RAF by CNK in *Drosophila*. *EMBO J* 22:5068–5078.